

Impact of assimilating IASI radiance observations on forecasts of two tropical cyclones

Dongmei Xu · Zhiquan Liu · Xiang-Yu Huang ·
Jinzhong Min · Hongli Wang

Received: 3 December 2012 / Accepted: 20 August 2013 / Published online: 31 August 2013
© The Author(s) 2013. This article is published with open access at Springerlink.com

Abstract The impact of assimilating Infrared Atmospheric Sounding Interferometer (IASI) radiance observations on the analyses and forecasts of Hurricane Maria (2011) and Typhoon Megi (2010) is assessed using Weather Research and Forecasting Data Assimilation (WRFDA). A cloud-detection scheme (McNally and Watts 2003) was implemented in WRFDA for cloud contamination detection for radiances measured by high spectral resolution infrared sounders. For both Hurricane Maria and Typhoon Megi, IASI radiances with channels around 15- μm CO₂ band had consistent positive impact on the forecast skills for track, minimum sea level pressure, and maximum wind speed. For Typhoon Megi, the error reduction appeared to be more pronounced for track than for minimum sea level pressure and maximum wind. The sensitivity experiments with 6.7- μm H₂O band were also conducted. The 6.7- μm band also had some positive impact on the track and minimum sea level pressure. The improvement for maximum wind speed forecasts from the 6.7- μm band was evident, especially for the first 42 h. The 15- μm band consistently improved specific humidity forecast and we found improved temperature and horizontal wind forecast on most levels. Generally, assimilating the 6.7- μm band degraded forecasts, likely indicating the inefficiency of the current WRF model and/or data

assimilation system for assimilating these channels. IASI radiance assimilation apparently improved depiction of dynamic and thermodynamic vortex structures.

Abbreviations

3DVAR	Three-dimensional variational
4DVAR	Four-dimensional variational
AIRS	Advanced InfraRed Sounder
AMSU	Advanced Microwave Sounding Unit
AVHRR	Advanced Very High Resolution Radiometer
CMA	China Meteorological Administration
CrIS	Cross-Track Infrared Sounder
CRTM	Community Radiative Transfer Model
ECMWF	European Centre for Medium-Range Weather Forecasts
EUMETSAT	European Organisation for the Exploitation of Meteorological Satellites
GFS	Global Forecast System
GTS	Global Telecommunication System
IASI	Infrared Atmospheric Sounding Interferometer
MetOp	Meteorological Operation
NCAR	National Center for Atmospheric Research
NCEP	National Centers for Environmental Prediction
NHC	National Hurricane Center
NOAA	National Oceanic and Atmospheric Administration
NWP	Numerical Weather Prediction
RRTM	Rapid Radiative Transfer Model
WRF	Weather Research and Forecasting model
WRFDA	WRF Data Assimilation
YSU	Yonsei University

Responsible Editor: C. Simmer.

D. Xu · J. Min
University of Information Science and Technology, Nanjing,
China

D. Xu · Z. Liu · X.-Y. Huang (✉) · H. Wang
National Center for Atmospheric Research, 3450 Mitchell LN,
Boulder, CO 80301, USA
e-mail: huangx@ucar.edu

1 Introduction

As part of the European Organisation for the Exploitation of Meteorological Satellites' (EUMETSAT) European Polar System (Blumstein et al. 2004), Infrared Atmospheric Sounding Interferometer (IASI) provides observational data with unprecedented accuracy and resolution on atmospheric temperature and humidity. IASI measures the radiances emitted from the Earth in 8,461 channels covering the spectral interval $645\text{--}2,760\text{ cm}^{-1}$ at a resolution of 0.5 cm^{-1} (apodized) and with a footprint of 12 km at nadir.

IASI observations from Meteorological Operation (MetOp)-A were declared operational by EUMETSAT on 27 July 2007. Since July 2008, the data have been operationally assimilated in the French global model, and since April 2010 in the French convective-scale model (Guidard et al. 2011). The impact of the assimilation of clear-sky IASI radiance on forecast skill is found to be positive for both models. Collard and McNally (2009) evaluated the quality of the IASI radiances by comparing measured radiance spectra with values computed from the ECMWF short-range forecasts in the passive data monitoring stage. Their study suggested that the IASI observations were comparable or even superior in quality to those of Advanced InfraRed Sounder (AIRS) channels in terms of bias and standard deviation.

Although major Numerical Weather Prediction (NWP) centers evaluated the impact of the IASI radiance assimilation on global and regional operational forecast skills, there are few studies that have directly explored the ability of regional models and data assimilation (DA) systems to ingest IASI radiances in tropical cyclone (TC) forecasts. Satellite radiance data are currently assimilated at major operational NWP centers and these data are important for global NWP operations, especially over areas with sparse conventional observations (e.g., Prasad et al. 1998; McNally et al. 2000; Zapotocny et al. 2008). TC track and intensity forecast error reductions are largely attributed to general advancements in TC initialization, DA techniques, and the assimilation of more observations, particularly those from satellite platforms (e.g., Li and Liu 2009; Liu et al. 2012; Schwartz et al. 2012). IASI radiance observations are found to be of high quality with high resolution, thus positive impact from IASI radiances DA is expected for TC forecasts. In this study, we implement the IASI radiance DA capability into WRFDA (Barker et al. 2012) and evaluate its impact on TC forecasting.

Due to the large uncertainty of modeling the hydrometeors in NWP and inaccuracy of Radiative Transfer Model (RTM) to simulate the cloudy radiance, it is difficult to assimilate infrared sounding radiances in the presence of cloud. Most NWP centers and researchers concentrate on the assimilation of clear-sky radiances (e.g., McNally et al.

2006; Collard and McNally 2009). Cloud detection, as part of quality control procedures to reject cloud-affected radiances, is crucial for proper assimilation of clear-sky radiances from infrared sounders. This work implements a cloud-detection scheme (McNally and Watts 2003) in WRFDA. This scheme is designed to determine the channels from the high spectral resolution infrared sounders—AIRS, IASI, and Cross-Track Infrared Sounder (CrIS), free of cloud at a given location for the purposes of radiance DA, which is used operationally at the European Centre for Medium-Range Weather Forecasts (ECMWF). Differing from traditional infrared cloud-detection scheme discarding all channels when cloud is present, this scheme attempts to detect and keep channels unaffected by cloud at a given location, thereby retaining as much information as possible from radiance observations in these cloudy areas.

As the first attempt to assimilate the IASI radiances in WRFDA (Barker et al. 2012) system, the impact of IASI radiance assimilation was evaluated for Hurricane Maria (2011) and Typhoon Megi (2010) forecast skills by using the 3-dimensional variational (3DVAR) component of WRFDA (Barker et al. 2004), which is technically more mature (at the time of this study being conducted) than other WRFDA options such as 4-dimensional variational (4DVAR: Huang et al. 2009) and ensemble-based techniques (e.g., Wang et al. 2008; Liu et al. 2012; Schwartz et al. 2012, 2013). The rest of this paper is as follows. In Sect. 2, we provide a brief introduction to the WRFDA system, radiance assimilation methodology, and cloud detection. An overview of Hurricane Maria and Typhoon Megi is described in Sect. 3. Section 4 gives the experimental setting. Results are presented in Sect. 5 before concluding in Sect. 6.

2 Assimilating IASI radiances with WRFDA

2.1 WRFDA

The WRFDA system developed at the National Center for Atmospheric Research (NCAR) includes 3DVAR, 4DVAR, and hybrid DA techniques (Barker et al. 2012). We employ the 3DVAR component of WRFDA in this study. The basic goal of variational data assimilation is to obtain a statistically optimal estimate of the true atmospheric state at a desired analysis time through an iterative minimization of the prescribed cost function $J(\mathbf{x})$ (Ide et al. 1997),

$$J(\mathbf{x}) = \frac{1}{2}(\mathbf{x} - \mathbf{x}_b)^T \mathbf{B}^{-1}(\mathbf{x} - \mathbf{x}_b) + \frac{1}{2}(\mathbf{y} - H(\mathbf{x}))^T \mathbf{R}^{-1}(\mathbf{y} - H(\mathbf{x})), \quad (1)$$

where \mathbf{x} is the atmospheric state vector, \mathbf{x}_b the background state (usually a short-range forecast), H the nonlinear

observation operator, and \mathbf{y} the observation vector. \mathbf{B} and \mathbf{R} are the background and observation error covariance matrices, respectively. If an iterative solution of \mathbf{x} can be found by minimizing (1), the result represents a minimum variance estimate of the true atmospheric state, given the background \mathbf{x}_b and observation \mathbf{y} , as well as \mathbf{B} and \mathbf{R} (Lorenz 1986). The conjugate gradient method is used to minimize the incremental cost function. A detailed description of this system can be found in Barker et al. (2004).

2.2 Radiance assimilation methodology

For assimilating radiance data, the Community Radiative Transfer Model (CRTM) (Han et al. 2006; Liu and Weng 2006) built in WRFDA (Barker et al. 2012) is used as the observation operator for computing radiance from the model profiles of temperature and moisture. In this study, we use a subset of 616 channels, which are pre-selected by National Centers for Environmental Prediction (NCEP) from all 8,461 channels in MetOp-A IASI radiances.

Figure 1 displays the observed brightness temperature (BT) and the calculated background BT, using CRTM for a clear-sky pixel. CRTM-calculated radiances are generally in good agreement with the observed values. However, large difference is seen for O_3 -sensitive channels around $9.6 \mu\text{m}$ and short-wave channels ($<4.4 \mu\text{m}$). Note that the WRF model does not predict O_3 (Skamarock et al. 2008), thus no O_3 profiles were used in CRTM in the above calculations. These channels are excluded in this study as in the current practice of major operational centers (e.g., Guidard et al. 2011). Channels with high-peaking weighting functions (near or above the model top) are also removed. Water vapor channels around $6.7 \mu\text{m}$ are not

currently assimilated at operational centers, but preliminary testing of these channels was performed in our study. Therefore, 300 channels (160 channels around $15 \mu\text{m}$ and 140 channels around $6.7 \mu\text{m}$) were selected before applying cloud detection (flagged with black dots in Fig. 1).

Radiances are prone to systematic errors (i.e., biases) that must be corrected before they are assimilated (Dee and Uppala 2009). Liu et al.'s (2012) modified observation operator is as follows:

$$\tilde{H}(\mathbf{x}, \beta) = H(\mathbf{x}) + \beta_0 + \sum_{i=1}^{I_p} \beta_i p_i(\mathbf{x}). \quad (2)$$

The modified observation operator \tilde{H} includes corrections to the model-simulated brightness temperatures based on β_0 (constant component of total bias), I_p potentially state-dependent predictors p_i and their coefficients β_i , which are assumed to be channel dependent (Eyre 1992) and can be estimated offline (Harris and Kelly 2001) or updated within a variational minimization process by inclusion in the control variables (Derber and Wu 1998; Dee and Uppala 2009; Auligné et al. 2007). The latter method is referred to as variational bias correction (VarBC), which we use in this study. The predictors of Eq. (2) used in the WRFDA/VarBC include seven parameters: the scan position, the square and cube of scan position, 1,000–300 hPa and 200–50 hPa layer thicknesses, surface skin temperature, and total column water vapor. A radiance observation is rejected if the bias-corrected innovation (observation minus prior) exceeds either 15 K or $3\sigma_o$, where σ_o is the specified observation error standard deviation for brightness temperature.

Fig. 1 Selected channels (black dots), observed (red line), and CRTM-calculated (blue dashed line) brightness temperatures (Units: K) for a clear-sky pixel at (lat = -7.2 , lon = -141.14) at 0000 UTC 19 October 2010

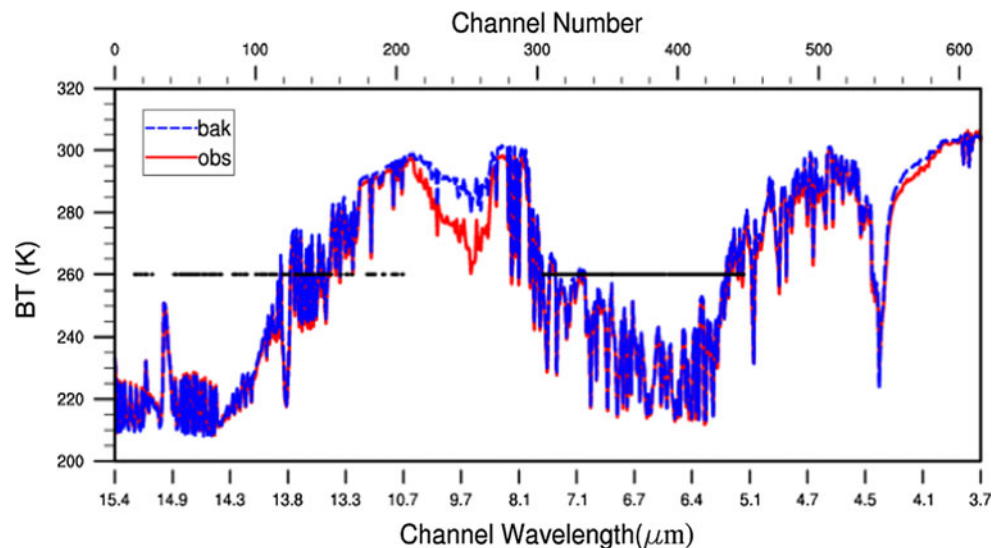


Table 1 Thresholds for the cloud detection (see “Appendix” for explanation)

	Default settings	New thresholds
BT_Threshold	0.5	4
BT_Grad_Threshold	0.02	0.06

2.3 Cloud detection

Detecting channels unaffected by cloud according to their characteristic levels allows a better use of available data and avoid discarding potentially useful information. A robust channel-based (instead of pixel-based) cloud-detection scheme is essential for efficient infrared radiance assimilation.

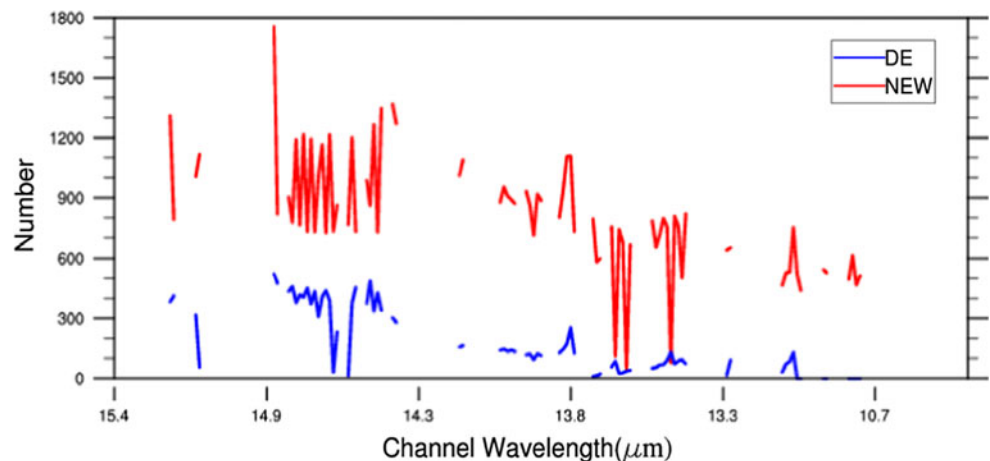
The cloud-detection algorithm developed by McNally and Watts (2003) takes the clear-sky first-guess departures as input and looks for the lowest model level above which the atmosphere is free of the cloud. This cloud-detection algorithm is adopted by ECMWF and briefly described in “Appendix”. The thresholds used at ECMWF and in this study are listed in Table 1. The new thresholds given were based on sensitivity tests and we found that the cloud-detection scheme can be largely affected by tuning parameters (the optimal tuning is beyond the scope of this paper). Figure 2 shows the number of radiance observations detected as clear after cloud detection with the default thresholds in ECMWF and new thresholds in Table 1, at 1800 UTC 14 September 2011. While the cloud detection with default (more strict) thresholds resulted in too many data being rejected, using new thresholds led to more observations being assimilated.

One may use the cloud detection in one spectral band to infer cloudy channels in another band (called cross-band option). Five bands are defined covering the 15- μm CO_2 absorption band, the O_3 absorption band, the 6.7- μm H_2O absorption band, the long-wave side of the 4.3- μm CO_2

absorption band, and the short-wave side of the 4.3- μm CO_2 absorption band. In this study, the algorithm is applied to the individual CO_2 band in finding the level at which cloud no longer affects the observed BT. This level is then used to determine the cloudy channels in the H_2O band.

Figures 3 and 4 show the distribution of the pixels detected as clear after cloud detection for two channels at 1800 UTC 14 September 2011 (for Hurricane Maria) and at 1200 UTC 18 October 2010 (for Typhoon Megi). Here, we choose the channel 646 ($\sim 12.4 \mu\text{m}$) to represent lower-peaking channels with characteristic level around 850 hPa (Figs. 3a, 4a), the channel 299 ($\sim 13.89 \mu\text{m}$) with characteristic level around 200 hPa (Figs. 3b, 4b) to represent higher-peaking channels, and the channel 3527 ($\sim 6.55 \mu\text{m}$) with characteristic level around 400 hPa (Figs. 3c, 4c) to represent the channels in H_2O band. Figure 3d shows the distribution of the pixels detected as clear using default settings in ECMWF in cloud detection for the same channel in Figs. 3b and 4b (channel 646, with characteristic level around 200 hPa). With the default thresholds, there were very few data left even for this high-peaking channel (Fig. 3d). As expected, the cloud-detection scheme rejected more pixels for the lower-peaking channel than for the higher-peaking channel. The Advanced Very High Resolution Radiometer (AVHRR) cloud mask and the brightness temperature from FY-2 (the Chinese series of geosynchronous meteorological satellites—Feng Yun) were used to evaluate the performance of the cloud detection (shaded in Figs. 3a, 4a). Lower magnitude of brightness temperature indicates existence of higher cloud. There is a reasonable correspondence between areas that appear cloudy from these products and places where the IASI channels are identified cloudy by the cloud detection. It was evident for most areas where it appeared cloudy from cloud product, the lower-peaking channel (even the higher-peaking channel in some places) had been identified as cloudy as well. However, there were

Fig. 2 The number of observations used after cloud detection with new thresholds in Table 1 (red line); and with the default thresholds in Table 1 (blue line) at 1800 UTC 14 September 2011



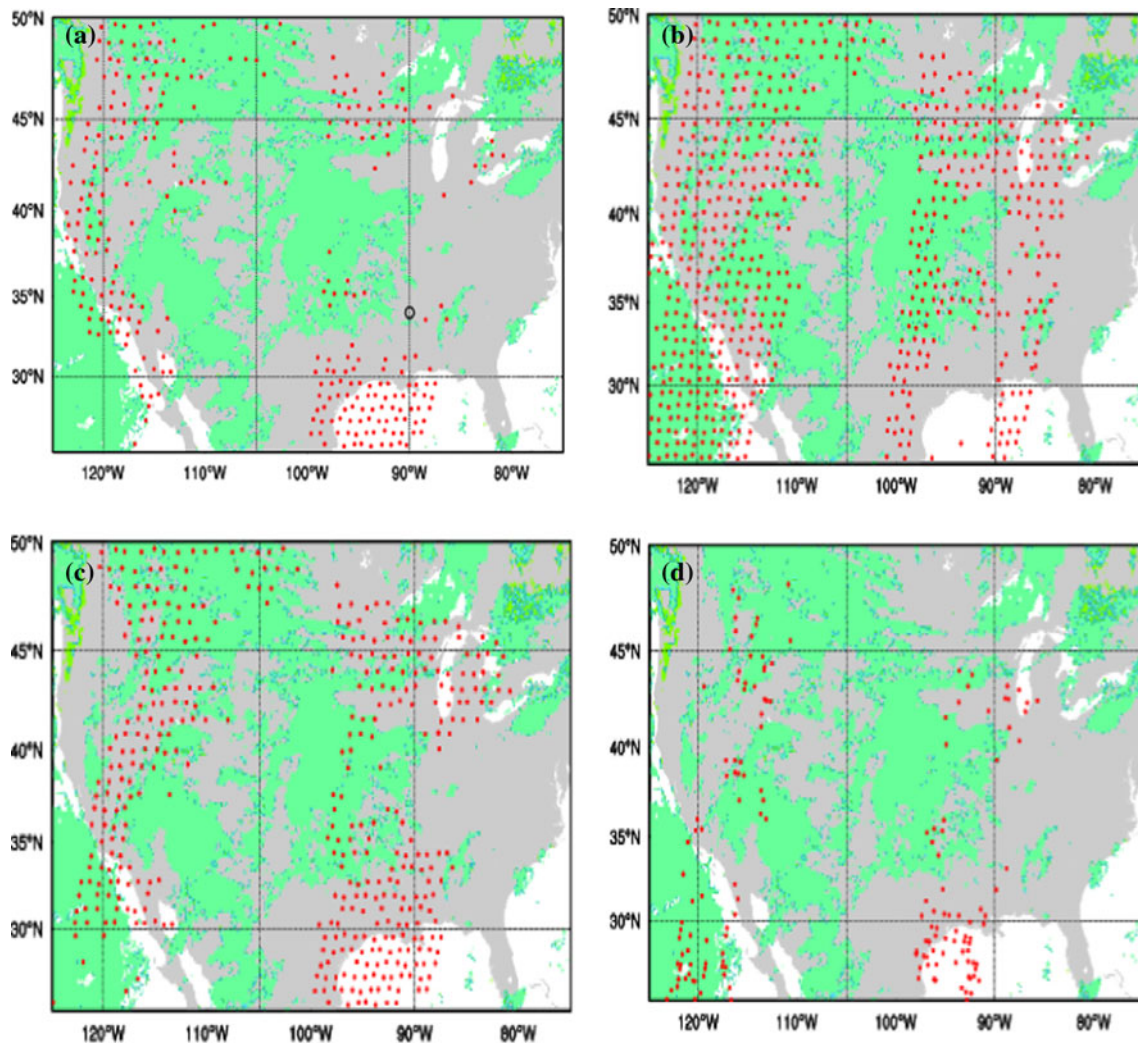


Fig. 3 For Maria, distributions of pixels identified as clear after cloud detection overlaid on the AVHRR cloud mask (shaded as cloudy) at 1800 UTC 14 September 2011 for **a** the channel 646 (wavelength: around 12.4 μm ; wavenumber: 806.25); **b** the channel 299

(wavelength: around 13.89 μm ; wavenumber: 719.5) in CO_2 band with new thresholds in Table 1; **c** channel 3527 (wavelength: around 6.55 μm ; wavenumber: 1,526.5) in H_2O band; and **d** the channel 299 with the original thresholds in Table 1

still areas where the scene was clear from the cloud products (e.g., the areas in the vicinity of the black circles in Figs. 3a, 4a), but the lower-peaking channel had been flagged cloudy. This may be caused by the scheme's misinterpretation for an error in the skin temperature provided by the NWP model, as cloud. Similar problems were also met by other researchers (e.g., McNally and Watts 2003). The higher-peaking channel was less sensitive to the surface emission and the clear locations from cloud image had a relatively better correspondence with clear-flagged pixels.

3 Overview of tropical cyclone cases

This study selected Hurricane Maria (2011) and Typhoon Megi (2010) to explore the impact of IASI radiances on

typical tropical cyclones in Atlantic and Pacific. Both events experienced two periods of strength and reached super hurricane (typhoon) intensity before landfall (Fig. 5).

Maria formed in the eastern Atlantic Ocean and quickly moved west-northwestward to the south of a subtropical ridge on 7 September 2011. By 9 September, Maria lost definition of the low-level circulation. Maria then turned northwestward, while its forward speed increased by 0000 UTC on 14 September. The cyclone slowly strengthened on 14 September and turned northward by 15 September. Maria then became a category 1 hurricane as it recurved through the northwestern Atlantic before making landfall in Newfoundland as a strong tropical storm around 1830 UTC 16 September. The experiments for the Maria case start on 12 September 2011 and end on 16 September 2011.

Megi was first identified on 12 October 2010 as a tropical disturbance roughly 90 km southeast of Guam. It attained

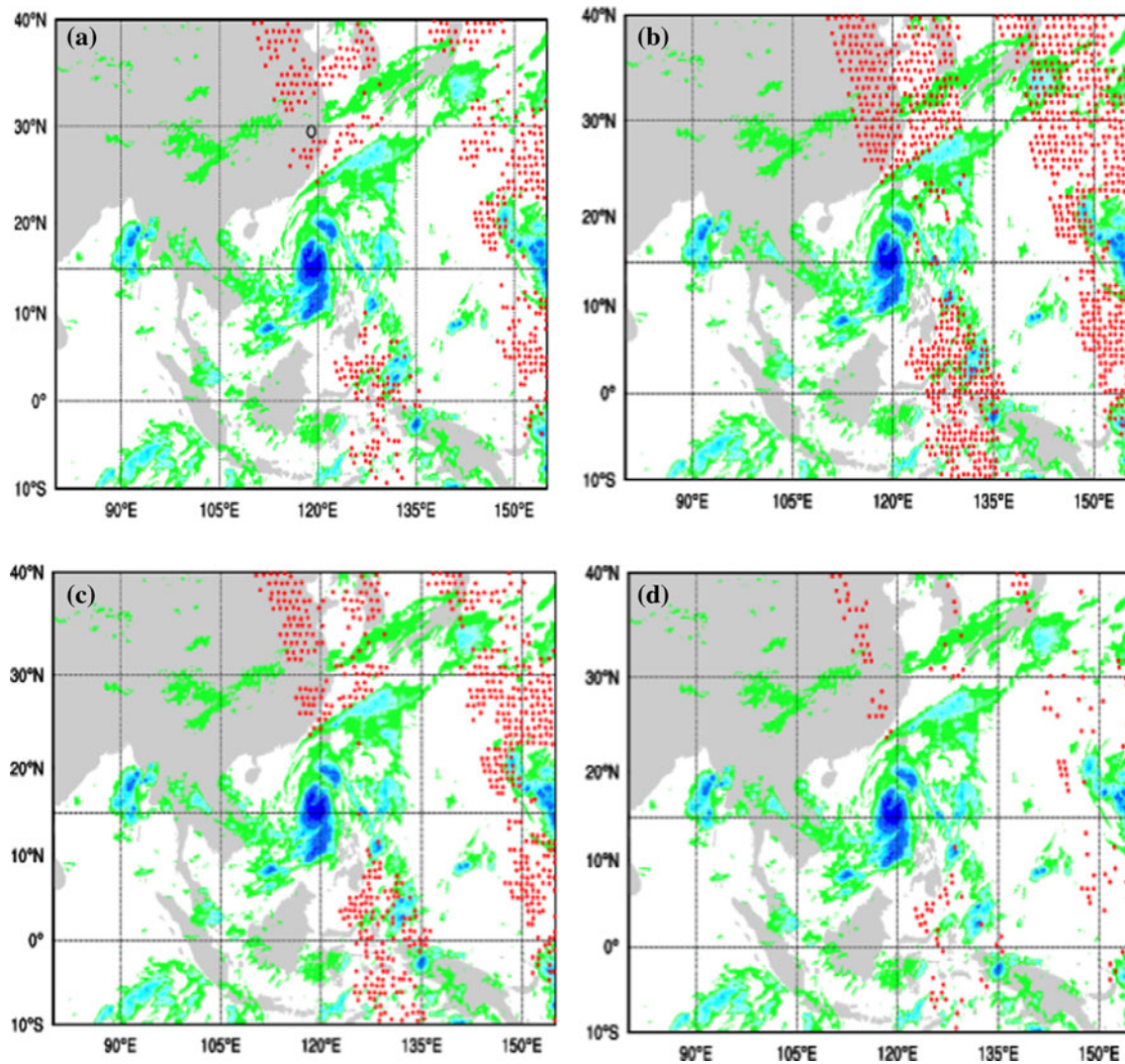


Fig. 4 For Megi, distributions of pixels identified as clear after cloud detection overlaid on the brightness temperature (Units: °C) from FY-2 at 1200 UTC 18 October 2010 for **a** the channel 646; **b** the channel

299; and **c** the channel 3527 in H₂O band; and **d** the channel 299 with the original thresholds in Table 1

winds just below typhoon status the next day. On 15 October, Megi was upgraded to a typhoon. On 16 October, Typhoon Megi gradually strengthened as it started to turn westward. Early on 17 October, Megi started to turn west–southwest and strengthened to a category 5 super typhoon. Megi made its first landfall over northeastern Luzon Island at 03:25 UTC on 18 October. Then, Megi weakened but quickly regained strength in the South China Sea, before weakening and losing its eyewall in the Taiwan Strait. Megi made its second landfall over Zhangpu in Fujian province, China on 23 October. After the landfall, Megi weakened to a tropical storm and further weakened to a tropical depression on 23 October. On 24 October, the remnant of Megi dissipated completely. This study focuses on the period when Megi regained the second strength before the landfall from 18 October 2010 to 23 October 2010.

4 Experiment setup

The model domain for Maria experiments, as shown in Fig. 5a, has a 15-km grid spacing on 718×373 horizontal grids and 43 vertical levels with the model top at 30 hPa. The model domain for Megi experiments, as shown in Fig. 5b, has a 36-km grid spacing on 215×156 horizontal grids and 43 vertical levels with the model top at 30 hPa.

For both cases, WRFDA/3DVAR either assimilated a control set of observations without IASI radiances or assimilated the control observations with IASI radiances. Four experiments, denoted as CTRL, IASI, IASI_WV, and IASI_DE, were conducted for both cases. The experiments are designed to examine the impact of IASI radiances (channels around 15 μm and around 6.7 μm) on analyses and the subsequent forecasts. The first experiment, CTRL,

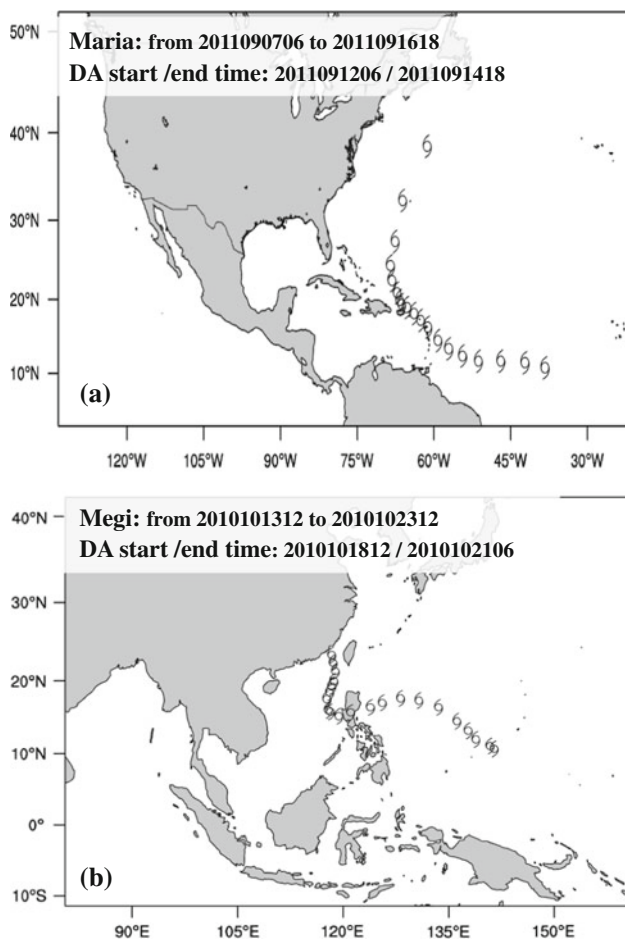


Fig. 5 The domains and best-track positions plotted every 12 h for **a** Maria from 0600 UTC 7 September 2011 to 1800 UTC 16 September 2011 with 15 km grid spacing; **b** Megi from 1200 UTC 13 October 2010 to 1200 UTC 23 October 2010 with 36 km grid spacing

assimilated conventional observations from the National Centers for Environmental Prediction (NCEP) operational Global Telecommunication System (GTS) dataset, and AMSU-A radiances from NOAA-15, 16, 18. The second experiment, IASI, assimilated all observations from CTRL plus IASI radiances with channels around $15.0\ \mu\text{m}$ from MetOp-A satellite. The third experiment “IASI_WV”, similar to IASI, also included water vapor channels around $6.7\ \mu\text{m}$. Two experiments IASI and IASI_WV used the new thresholds of cloud detection in Table 1. An additional experiment “IASI_DE”, similar to IASI but using the default thresholds in Table 1, was conducted to evaluate the performance of the new thresholds.

The 6-h cycling forecast-analysis experiments are carried out for both cases. For Maria, the data assimilation period begins at 0600 UTC 12 September and ends at 1800 UTC 14 September 2011. The background in the first analysis at 0600 UTC 12 September is provided by a forecast initiated from NCEP Global Forecast System (GFS) $1^\circ \times 1^\circ$ analysis at 0000 UTC 12 September 2011.

For the following cycles, the background is 6-h WRF forecast from the previous cycle. The lateral boundary conditions for the WRF forecasts are also provided by the operational GFS analyses at 3-h intervals. In total, there are 11 analyses and 11 48-h forecasts during the period.

We computed the background error statistics using the method from Parrish and Derber (1992). A set of cold-start forecasts was initiated from GFS analyses at 0000 and 1200 UTC every day from 12 August to 12 September 2011. We used the differences in the 24- and 12-h forecasts to derive the background error statistics.

The same cycling data assimilation and forecast configuration is taken for Megi. The analysis time starts at 1200 UTC 18 October 2010 and ends at 0600 UTC 21 October 2010. We also computed the background error statistics for the domain described above.

In these experiments, radiance (IASI and AMSU-A) data are used with a 90-km thinning mesh. Data within ± 2 h of analysis times were used and assumed to be valid at the analysis times. Radiance data over mixture surface (e.g., over coastal area) and observations with large scan angle (the first four pixels on the edge) are rejected.

WRF model (version 3.2.1) is employed in all forecast experiments. The following physical schemes are used: the WRF single-moment 5-class microphysics scheme (Hong et al. 2004); the Goddard shortwave (Chou and Suarez 1994) and Rapid Radiative Transfer Model (RRTM) longwave (Mlawer et al. 1997) radiation schemes, including the refined upper boundary condition for RRTM (Cavallo et al. 2011), which is necessary when cycling with model tops above 50 hPa; the Yonsei University (YSU) boundary layer scheme (Hong et al. 2006); the Noah land surface model (Chen and Dudhia 2001); and the Kain-Fritsch cumulus parameterization (Kain and Fritsch 1990).

5 Results

ECMWF is considered to be one of the best centers for TC track forecast (Fiorino 2009). ECMWF ERA-Interim (~ 79 km) reanalysis (Dee et al. 2011) (many more satellite data are assimilated with 4DVAR) were used in this study to assess large-scale features. The forecast skills of wind, temperature, and humidity were assessed by comparing the forecasts to ECMWF ERA-Interim reanalyses and conventional observations. The “best track”, minimum sea level pressure, and absolute maximum wind speed data for Hurricane Maria are from the National Hurricane Center (NHC) and the data for Typhoon Megi are from China Meteorological Administration (CMA). In addition, differences of analyses among the IASI, IASI_WV, and CTRL experiments were also illustrated to obtain further insight on the impact of IASI radiances.

5.1 Forecast verification against ERA-interim reanalyses

Figures 6 and 7 display vertical profiles of the 48-h forecast root mean square error (RMSE) for temperature, wind speed, and specific humidity, averaged over all cycle times for Maria and Megi, respectively. For Maria (Fig. 6), the 15- μm CO_2 band in IASI radiances improved temperature and specific humidity forecast consistently for all levels, and the improvement for horizontal wind forecast was observed at low levels. The assimilation of the 6.7- μm band in IASI_WV degraded forecasts for all variables at almost all levels, except for slightly positive impact on specific humidity forecast at 1,000 hPa. Note that the results from IASI_DE are nearly identical to those from CTRL because very few IASI radiances were assimilated after cloud detection.

Similar behavior is also observed for Typhoon Megi regarding the impact of IASI_DE, thus we show only the results from the CTRL, IASI, and IASI_WV experiments for the Megi (Fig. 7). The IASI experiment agreed better with the ERA-Interim reanalyses than the CTRL experiment for all variables at almost all levels. Adding water vapor channels in IASI_WV degraded temperature and wind forecasts at higher levels as compared to the IASI experiment, even though IASI_WV performed better than CTRL and as well as IASI for humidity and low level temperature and wind.

Impact of IASI radiances (temperature sensitive channels) on the wind and humidity forecast likely resulted from improved analyses that used multivariate correlations, as implied in the WRFDA/3DVAR background error covariance. This large impact on wind fields is consistent

with the results of Liu et al. (2012), when assimilating AMSU-A radiances using an Ensemble Kalman Filter for Atlantic Hurricanes and with the results of McNally (2007), when assimilating AIRS radiances.

5.2 Forecast verification against conventional observations

Similar to Figs. 6 and 7, Figs. 8 and 9 display similar RMSE profiles of the 48-h forecasts verified against a set of conventional observations (radiosondes and GeoAMV). Generally, verification results against conventional observations were consistent with verification versus ERA-Interim reanalyses. The CTRL experiment had the largest RMSE and IASI experiment had the smallest RMSE for temperature, wind, and specific humidity on most levels. For Maria, the scores of IASI and IASI_WV were comparable for temperature and specific humidity and IASI_WV degraded the wind forecast. Consistent with Fig. 6, IASI_DE with very few IASI radiances assimilated had RMSE much closer to CTRL, even though a smaller improvement was seen for temperature and wind. For Megi, the IASI_WV experiment degraded temperature and wind forecasts at most levels as compared to the IASI experiment.

5.3 Track and intensity forecast verification

To demonstrate how assimilation affects the TC forecasts, Fig. 10 shows the 48-h track forecasts of Maria initialized at 0600 UTC 13 September, 1800 UTC 13 September, 0600 UTC 14 October, and 1800 UTC 14 September, respectively. The best track positions from NHC (black

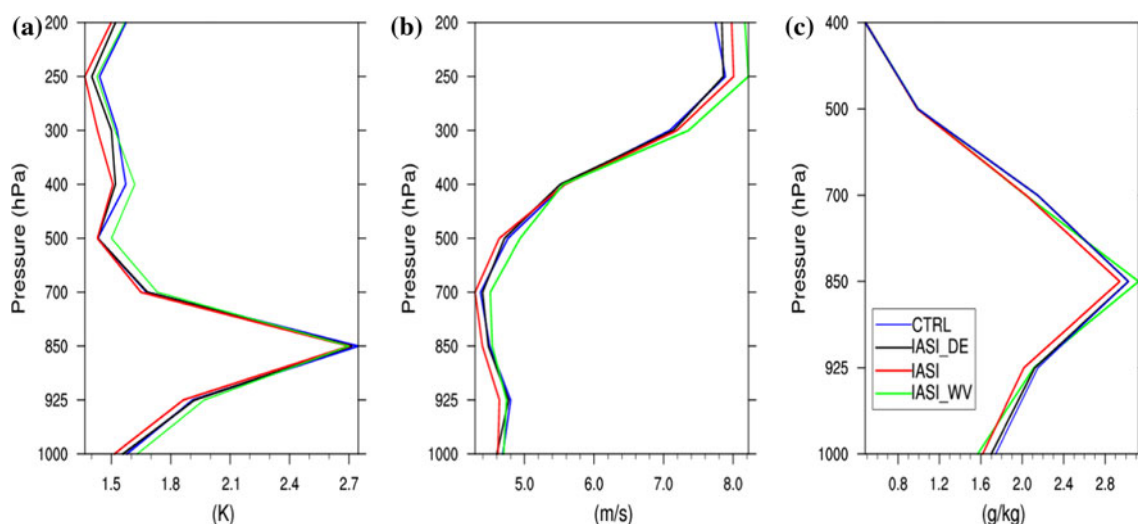


Fig. 6 For Maria, vertical profiles of 48-h forecast RMSE for **a** temperature; **b** wind speed; and **c** specific humidity, when compared to ERA-Interim reanalyses. Blue lines denote the results from the

CTRL experiment, black lines from IASI_DE, red lines from the IASI experiment, and green lines from IASI_WV

dot) are also plotted in Fig. 10. For the forecasts began at 0006 UTC 13 October (Fig. 10a), the forecast track from the IASI_WV experiment agreed better with the best track than did the CTRL and IASI experiments. The westward biases from the track of the CTRL experiment were significant, after 1800 UTC 13 September (Fig. 10b, c). IASI radiances prevented the track forecast from moving clearly westward, even though IASI and IASI_WV had slower movements. All predicted tracks moved slower than the best track did before landfall. Generally, there was no substantial difference between the track forecast from IASI and that from IASI_WV for most of the time. As expected,

IASI_DE's track forecasts were overall very close to those from CTRL.

Figure 11 shows the 48-h track forecasts of Megi initialized at 1200 UTC 19 October, 1800 UTC 19 October, 0600 UTC 20 October, and 0600 UTC 21 October, respectively. The best track positions from CMA (black dot) are also plotted in Fig. 11. For the forecasts beginning at 1200 UTC 19 October (Fig. 11a), the forecast track from the IASI experiment agreed better with the best track than did the CTRL experiment, especially after 0600 UTC 21 October, when IASI radiances prevented the track forecast from moving fast and northeastward. For the forecasts

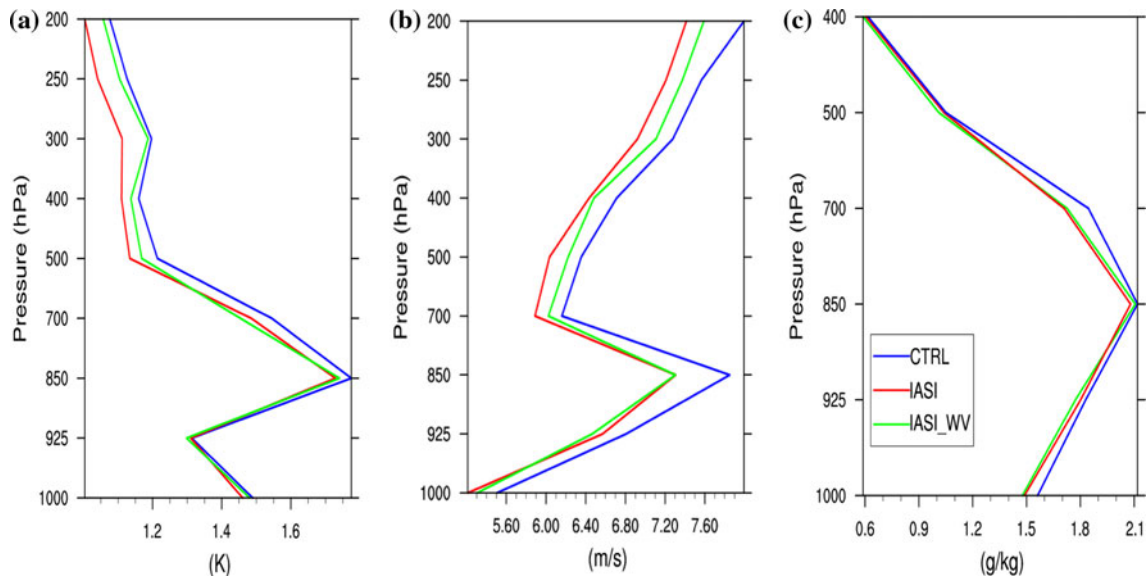


Fig. 7 Similar to Fig. 6, but for Megi. Blue lines the results from the CTRL experiment, red lines from the IASI experiment, and the green lines from the IASI_WV experiments

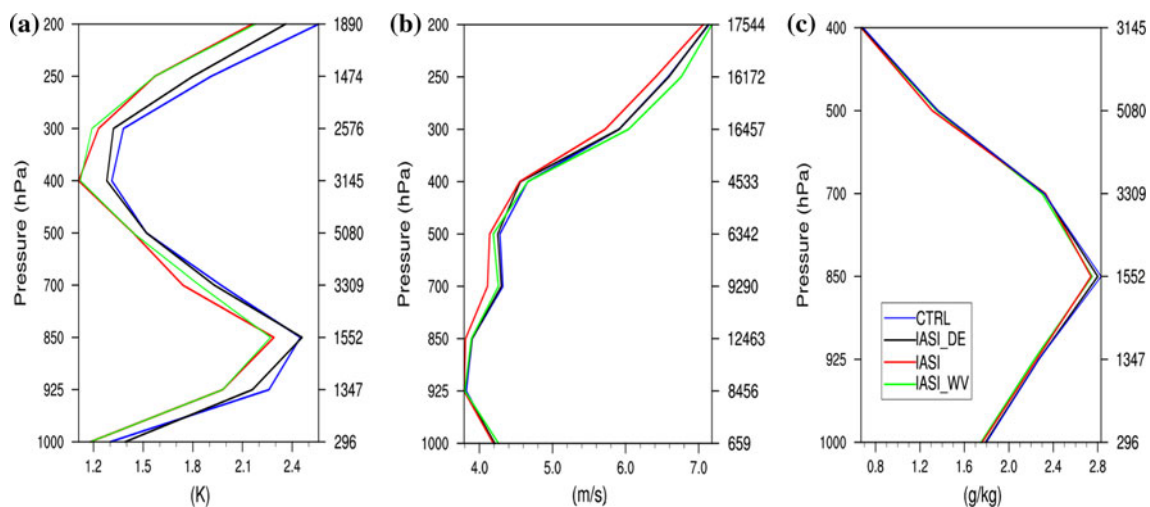


Fig. 8 For Maria, vertical profiles of 48-h forecast RMSE for **a** temperature; **b** wind speed; and **c** specific humidity, when compared to conventional observations. The number of conventional

observations is shown at the right of each panel. Blue lines the results from the CTRL experiment, black lines from IASI_DE, red lines from the IASI experiment, and green lines from IASI_WV

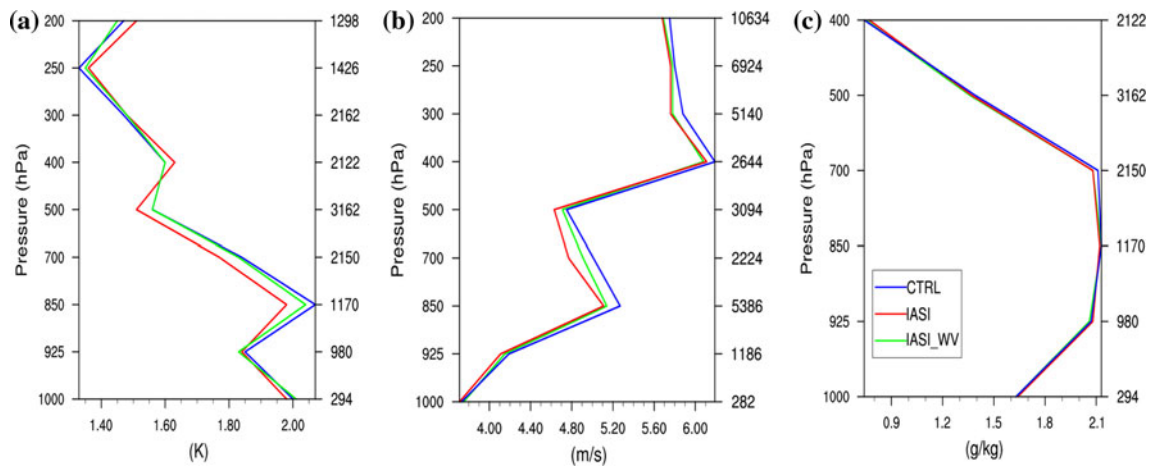
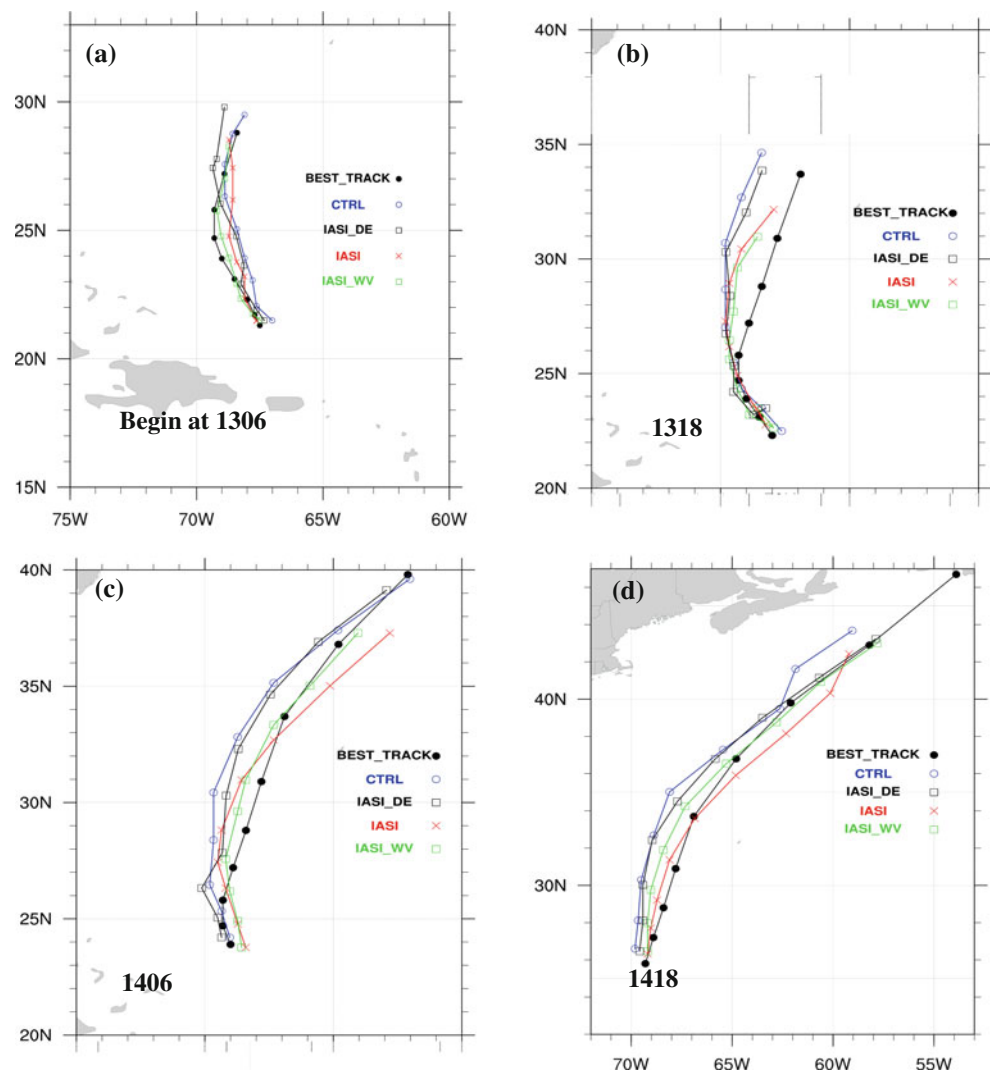


Fig. 9 Similar to Fig. 8, but for Megi. *Blue lines* the results from the CTRL experiment, *red lines* from the IASI experiment, and the *green lines* from the IASI_WV experiments

Fig. 10 For Maria, 48-h track forecasts initialized at **a** 0600 UTC 13 September 2011; **b** 1800 UTC 13 September 2011; **c** 0600 UTC 14 September 2011; and **d** 1800 UTC 14 September 2011, respectively



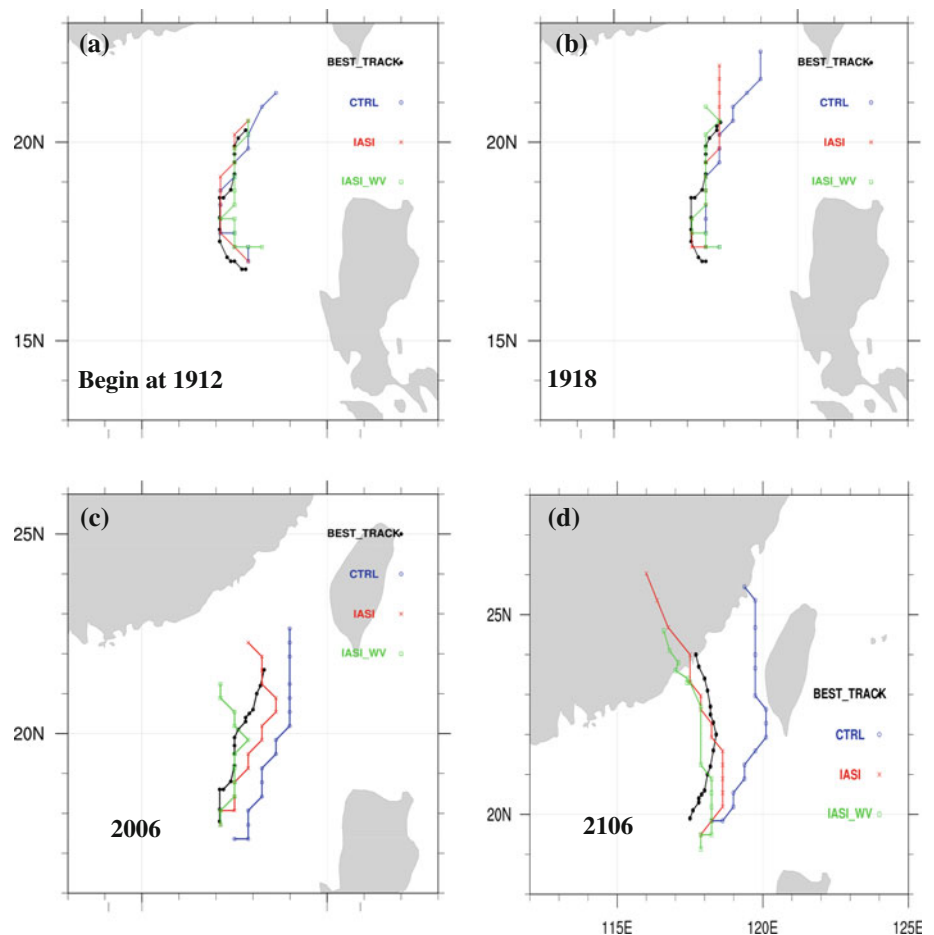
beginning at 1800 UTC 19 October (Fig. 11b), the eastward bias from CTRL experiment was more evident. The CTRL experiment had a significant northward bias and faster TC vortex movement around 1800 UTC 20 October. The eastward biases in the track forecast in the CTRL experiment were significant, for the forecasts beginning at 0600 UTC 20 October (Fig. 11c). For the forecast beginning at 0600 UTC 21 October (Fig. 11d), the IASI experiment had an overall consistent track with the best track, even though it had a faster movement. The forecast track difference between CTRL experiment and best track in Fig. 11d was significant. IASI_WV corrected the eastward bias of the track forecast from CTRL and prevented the track forecast from moving fast after 1800 UTC 19 October for the last 6 h. Track forecasts from IASI_DE were similar to those from CTRL (not shown).

Figure 12 displays the mean absolute track error, absolute maximum wind speed error, and minimum sea level pressure (MSLP) (average from all cycles) for Maria. We found that the reductions of the mean absolute track errors (~ 30 km smaller), maximum wind speed error (~ 3 m/s smaller), and the MSLP error (~ 3 hPa smaller) were obvious from both IASI and IASI_WV. Positive impact on

the track forecast lasted for 42 h. The $6.7\text{-}\mu\text{m}$ H_2O band brought additional positive impact on maximum wind. There was also small improvement for track from IASI_DE. Three experiments with IASI radiance DA performed very similar for MSLP forecasts.

Mean absolute track error, absolute maximum wind speed error, and MSLP (averaged over all cycles) as a function of forecast range for Megi are shown in Fig. 13. Consistent improvement (~ 20 km) on forecast track was achieved from analysis time to 48-h from experiments with IASI radiances, compared to that without IASI radiances (Fig. 13a). MSLP difference (Fig. 13c) between the experiments with IASI radiances and CTRL was evident for the first 24 h, with ~ 2 hPa smaller error from experiment with IASI radiances. IASI_WV brought additional positive impact on maximum wind for the first 36 h and on track forecast for the last 6 h. Positive impact on maximum wind speed from IASI was found from 9- to 42-h (Fig. 13b). Despite encouraging results regarding the TC intensity forecast improvement, intensity errors remained large because of coarse (36 km) model resolution used for the forecast, which is consistent with results from both Davis et al. (2010) and Liu and Rabier (2002).

Fig. 11 For Megi, 48-h track forecasts initialized at **a** 1200 UTC 19 October 2010; **b** 1800 UTC 19 October 2010; **c** 0600 UTC 20 October 2010; and **d** 0600 UTC 21 October 2010, respectively



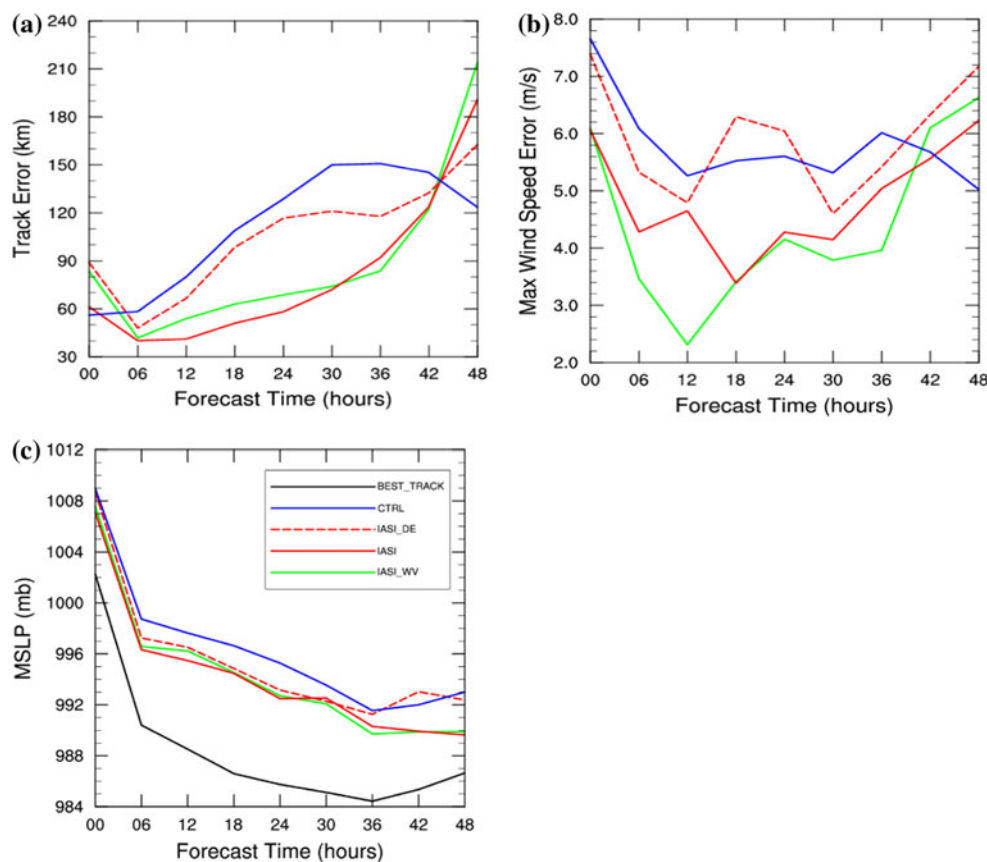
5.4 Impact on analyses

We show that IASI radiances reduced westward bias and eastward bias in track forecast for Maria and Megi, respectively. Past studies (e.g., Wang et al. 2011; Wang and Huang 2012) showed that wind perturbation around TC played an important role in TC movements. We examine the analysis differences between IASI and CTRL to identify possible causes that might lead to a better TC forecast, when IASI radiances are used. Figure 14 displays the time-averaged U-wind difference (shaded) between experiments (IASI-CTRL) at 700 hPa and those at 500 hPa. For Maria (Fig. 14a and b), the average is from 0600 UTC 12 September 2011 to 1800 UTC 14 September 2011. For Megi (Fig. 14c and d), the average is carried from 1200 UTC 18 October 2010 to 0600 UTC 21 October 2010 every 6 h. The averaged wind vector at 500 hPa in CTRL and the best track positions over the period are also plotted. From Fig. 14a and b, eastward (i.e., positive) U-wind increments are observed on two levels, which reduced westward bias in track forecast for Maria (see Fig. 10). From Fig. 14c, d, it can be seen that considerable westward (i.e., negative) U-wind increments along the typhoon track are found when assimilating IASI radiances on both levels. This wind increment drove Megi to recurve to the west compared to

the experiment without IASI radiances, as shown in track forecast (see Fig. 11).

Finally, we explore the impact of IASI data on the analyzed typhoon vertical structure. Figures 15 and 16 show the south-north vertical cross sections of potential temperature perturbation, horizontal wind speed fields, and in-plane flow, cutting across the analyzed hurricane center of Maria at 0600 UTC 13 September 2011 and the typhoon center of Megi at 0600 UTC 21 October 2010. An issue is that the model forecast vortex intensity is too weak (see, for example, Hsiao et al. 2010; Wang 2011; Zhao et al. 2012). This issue was noted in our study as well (Figs. 12c, 13c). In Fig. 15b, c, the IASI and IASI_WV experiments showed stronger presence of a trough in the potential temperature perturbation field, indicating clearer warm core structures. Figure 15c shows that IASI_WV resulted in an even more upright eyewall, and the strong tangential winds extended to a much higher level than IASI and CTRL do, which was consistent with the improvement of the maximum wind speed as shown in Sect. 5.2. Similarly, IASI data also had impact on the dynamic and thermodynamic vortex structure for Megi. The wind speed field in the IASI and IASI_WV experiments (Fig. 16b, c) exhibited tighter and circular typhoon circulations than that in the CTRL experiment (Fig. 16a), by increasing the wind speed

Fig. 12 For Maria, **a** mean absolute track errors; **b** mean absolute maximum wind speed errors; and **c** minimum sea level pressure as a function of forecast lead time. Blue lines the results from the CTRL experiment, red lines from the IASI experiment, and green lines for IASI_WV experiment. The average is over examples from 0600 UTC 12 September 2011 to 1800 UTC 14 September 2011



in the south side. Meanwhile, the potential temperature perturbation fields showed the presence of a trough around the typhoon center associated with the stronger typhoon structure in the IASI and IASI_WV experiments. The typhoon eye was much wider and the intensity was weaker in the CTRL experiment than in the IASI experiment. The wind speed from IASI_WV was slightly larger than that from IASI, especially at the height of 12 km.

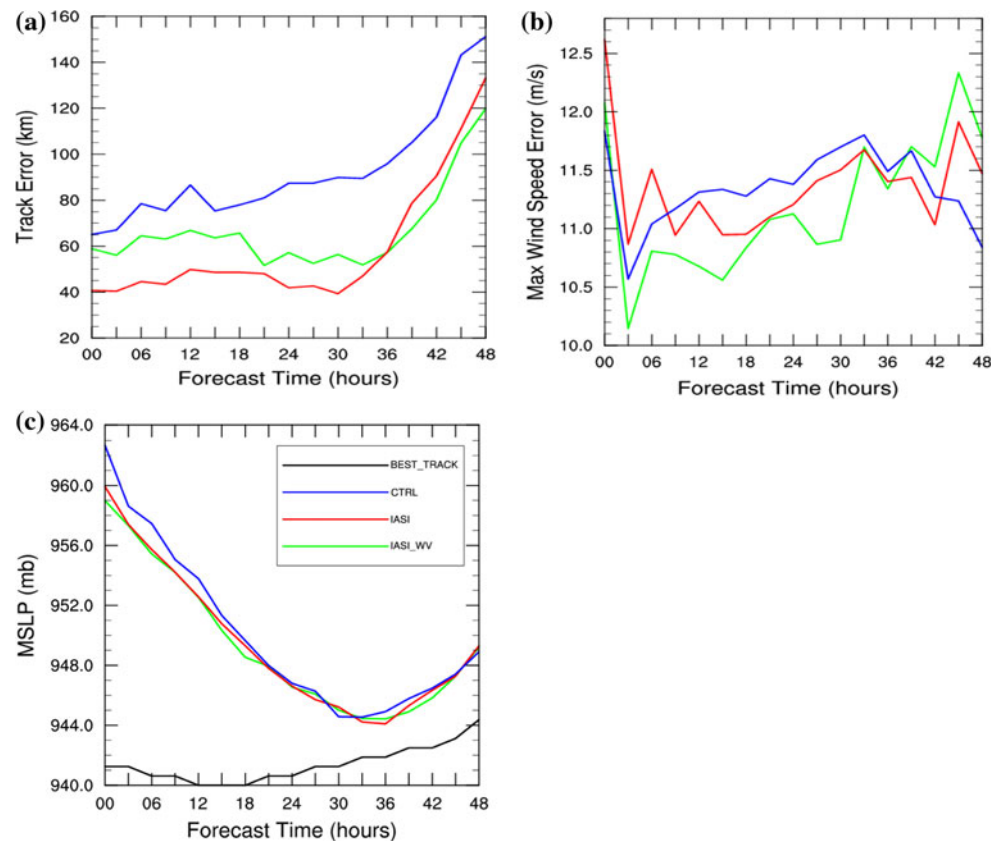
6 Summary and future perspectives

This study implemented the capability to assimilate the IASI radiances along with quality control within WRFDA. The cloud-detection procedure of McNally and Watts (2003) was added to WRFDA. This cloud-detection scheme was demonstrated to be effective based on the channel's characteristic levels in this study. With default more strict thresholds used in ECMWF, IASI radiances were over rejected and the results from IASI experiments were nearly identical to those from experiments without IASI radiances. The use of less stringent cloud-detection thresholds resulted in a much more reasonable amount of IASI data being assimilated. The impact of assimilating IASI radiances from the MetOp-A satellites on Hurricane

Maria and Typhoon Megi forecasts was evaluated. Assimilating the channels around 15 μm of IASI radiances brought the TC environmental fields closer to the ERA-Interim reanalyses and conventional observations. IASI radiance data prevented the east/west bias in track forecast for the Maria/Megi experiments, which likely resulted from the improvement for wind forecast and brought positive impact on the forecast skill for hurricane/typhoon minimum sea level pressure and maximum wind speed. While slightly positive and neutral impact was obtained for some aspects of verification metric, assimilating the 6.7- μm water vapor band generally degraded the forecasts, likely indicating the inefficiency of the current WRF model and/or WRFDA/3DVAR system in assimilating data from these channels. Finally, IASI radiance data apparently improved depiction of the dynamic and thermodynamic vortex structure.

In this study, we used WRFDA/3DVAR to investigate one hurricane and one typhoon. To assess the impact of IASI assimilation on tropical cyclones, additional studies with more cases over extended periods are needed. The 4DVAR component of WRFDA (Huang et al. 2009), when it becomes more mature, should be used to assess the impact of IASI data, as it can make better use of radiance data by assimilating these data at appropriate times.

Fig. 13 For Megi, **a** mean absolute track errors; **b** mean absolute maximum wind speed errors; and **c** minimum sea level pressure as a function of forecast lead time. Blue lines the results from the CTRL experiment, red lines from the IASI experiment. The average is over examples from 1200 UTC 18 October 2010 to 0600 UTC 21 October 2010



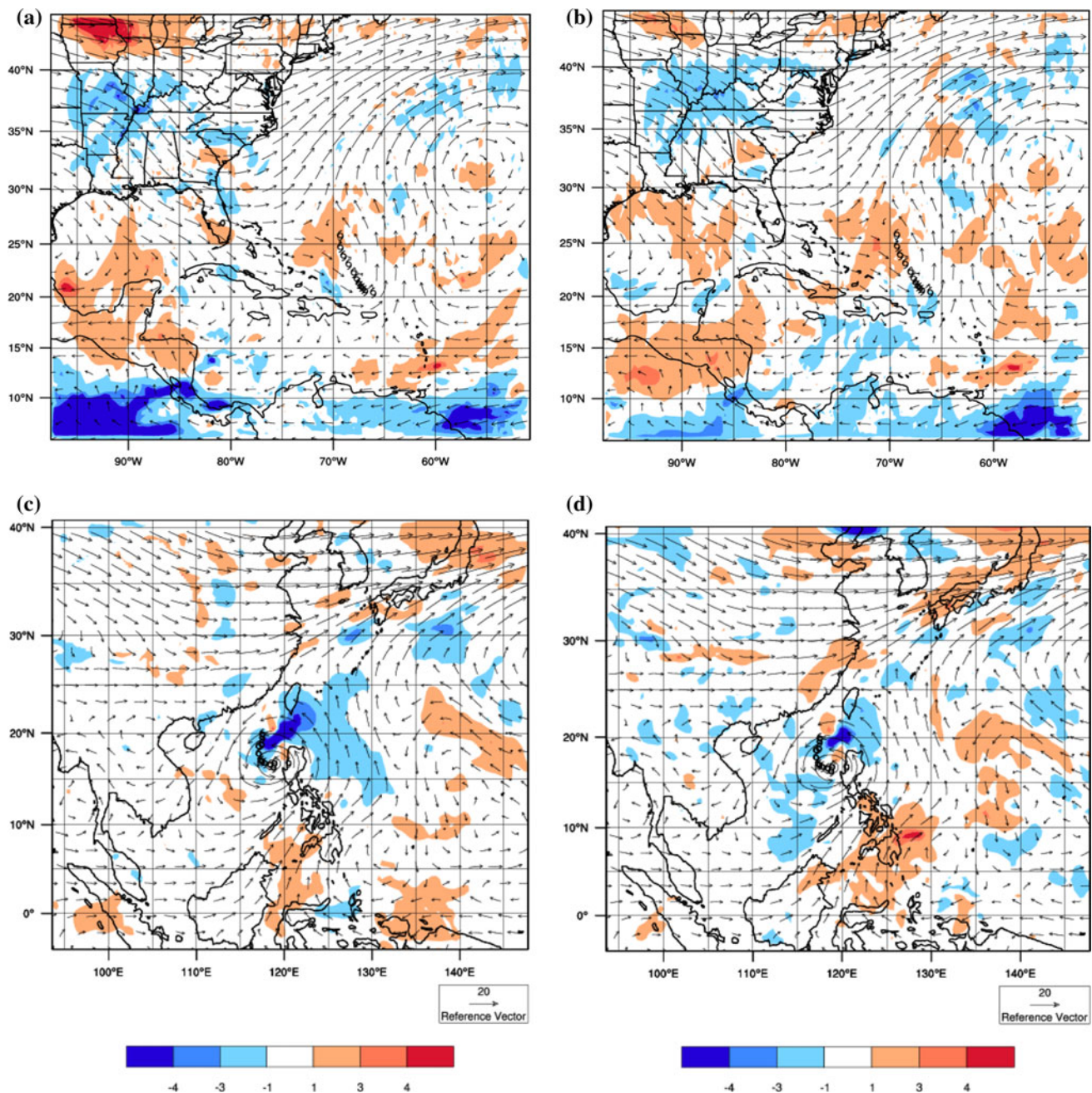


Fig. 14 The time-averaged U-wind (*shaded contours*) difference of analyses between IASI and CTRL experiments (Units: m/s) for **a** Maria at 700 hPa; **b** Maria at 500 hPa; **c** Megi at 700 hPa; and **d** Megi at 500 hPa. For Maria, the average is from 0600 UTC 12 September to 1800 UTC 14 September 2011 every 6 h. For Megi, the

average is carried out over 12 examples from 1200 UTC 18 October 2010 to 0600 UTC 21 October 2010 every 6 h. The average wind vectors at 500 hPa in CTRL and the best track positions over the period are overlaid

Ensemble/Var Hybrid DA (Wang et al. 2008; Schwartz et al. 2013) can use the ensemble to estimate the forecast error statistics in a flow-dependent manner, which can also be considered for future studies.

We found that the cloud-detection scheme (McNally and Watts 2003) was affected by the choice of thresholds. With default settings in ECMWF, the scheme over-rejects the data. Future work will likely address using adaptive

statistical thresholds to improve the performance of the cloud-detection scheme. The refinement of the assumed observation errors and the bias correction will be further explored to potentially increase the impact of IASI. Another issue is an efficient use of more channels of the entire IASI spectra. While the IASI channels in the 15- μm CO_2 band are in good use, future development on improvements in WRFDA and WRF may lead to a better

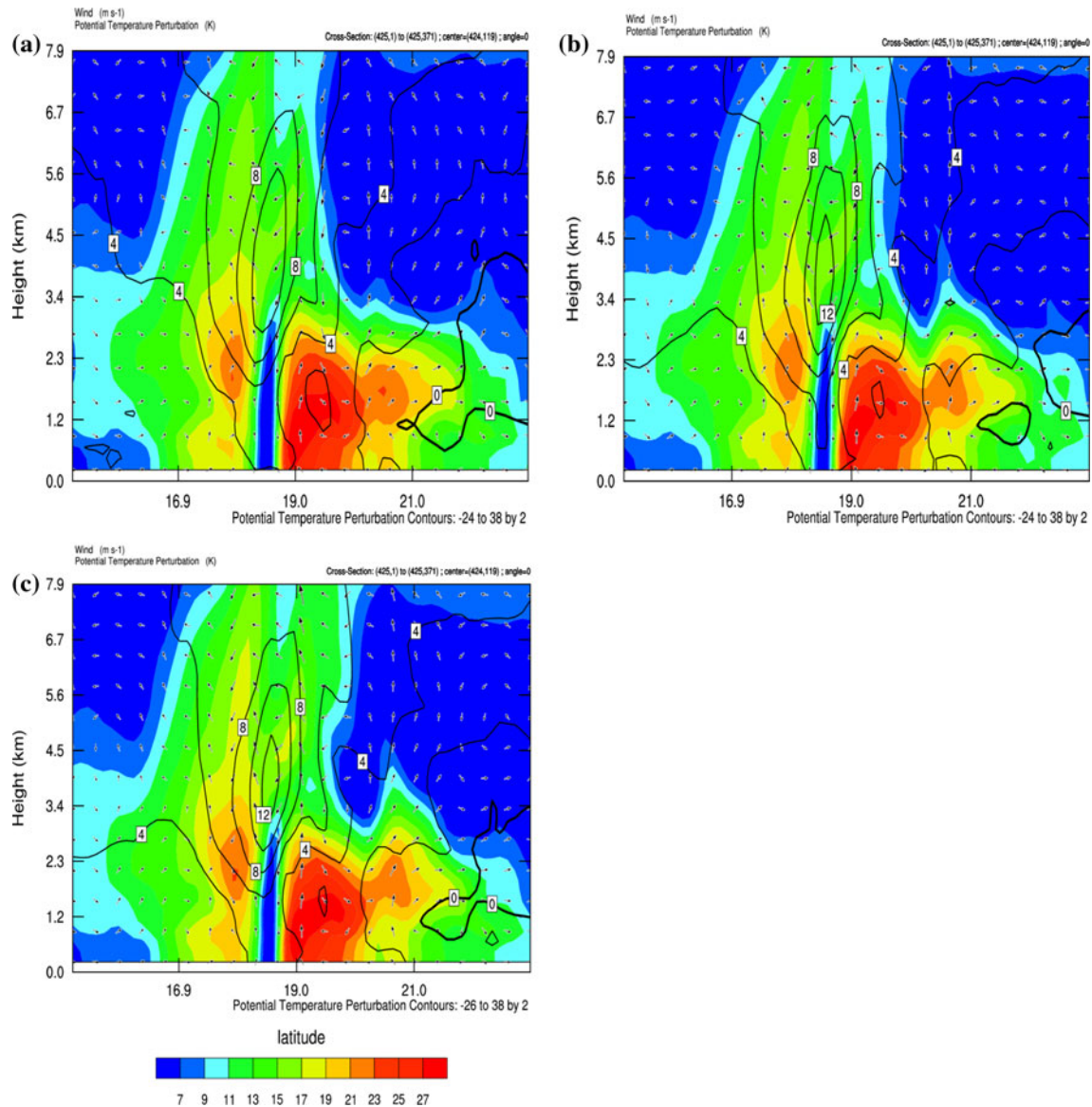


Fig. 15 For Maria: analyzed horizontal wind speed (interval of 2 m/s, *shaded*), potential temperature perturbation (interval of 5 K, *solid contours*), and in-plane flow (*vector*) in the south-north (from

use of channels around 6.7 μm . The high quality of prior background information from NWP model should allow more channels of IASI data to be used in future.

Acknowledgments This work was jointly sponsored by the 973 Program (2013CB430102), the National Natural Science Foundation of China (40975068), AirDat LLC (now Panasonic Weather Solutions) under Grant RAL10180 Task Order 20093005, and the Priority Academic Program Development of Jiangsu Higher Education Institutions (PAPD). The authors would like to thank the anonymous reviewers for their valuable comments on the earlier versions of the manuscript; Drs. Feng Gao, Peter Childs, Junmei Ban and Xin Zhang for fruitful discussions; and Steven T. Olson for editing the manuscript. The National Center for Atmospheric Research is sponsored by the National Science Foundation. Any opinions, findings, and conclusions or recommendations expressed in this publication are those of the

the grid point 0 to 372 for Maria shown in the x -axis) vertical cross-sections through the analyzed hurricane center for **a** CTRL; **b** IASI for Maria; and **c** IASI_WV for Maria at 1800 UTC 12 September 2011

author(s) and do not necessarily reflect the views of the National Science Foundation.

Open Access This article is distributed under the terms of the Creative Commons Attribution License which permits any use, distribution, and reproduction in any medium, provided the original author(s) and the source are credited.

Appendix: The cloud-detection algorithm

For detailed description of the cloud-detection algorithm, please refer to McNally and Watts (2003). Each channel is first assigned an altitude (or pressure). The characteristic level k for a channel is determined as the first point from

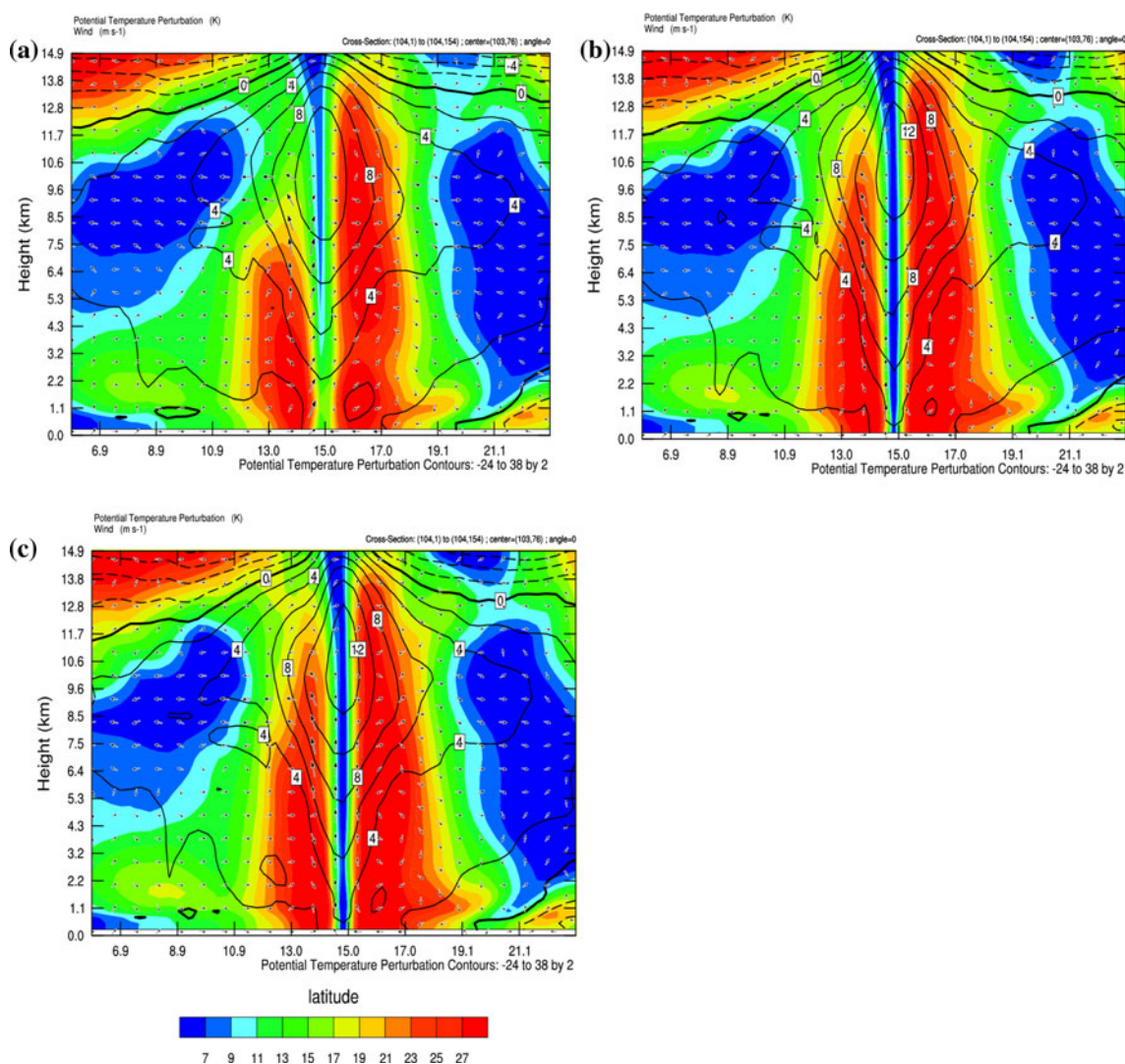


Fig. 16 For Megi: analyzed horizontal wind speed (interval of 2 m/s, shaded), potential temperature perturbation (interval of 5 K, solid contours), and in-plane flow (vector) in the south-north (from the grid

point 0 to 154 shown in the x -axis) vertical cross-sections through the analyzed typhoon center for **a** CTRL; and **b** IASI at 0600 UTC 21 October 2010

surface to top at which the relative impact of an opaque black cloud to the total clear-sky radiance is larger than 1 %, i.e.,

$$\frac{|R_v^0 - R_v^k|}{R_v^0} > 0.01, \quad (3)$$

where R_v^0 is the radiance computed by the radiative transfer model in clear sky for the channel number v and R_v^k is the radiance calculated for overcast black cloud at level k . This leads to ordering measures based on the low-altitude/high-pressure tail of the channel-weighting function $(\partial\tau(z, \infty)/\partial z)$, where τ is the transmittance between the height z and the top of atmosphere. Weighting function will determine how much one atmospheric layer contributes to the measured signal.

Then, the channels are ranked according to their heights, with the highest channels first and the channels closest to the surface last. The brightness temperature departure represents the difference between the observed BT and BT calculated from the clear-sky atmospheric. The ranked BT departures are smoothed with a moving-average filter to reduce the impact of instrument noise. The level at which cloud no longer significantly affects the radiances is found by stepping through the channels with increasing height until the observed minus calculated brightness temperature difference and local gradient fall below predetermined thresholds:

- (a) $|\text{BT departure}(i)| < \text{BT_Threshold}$;
- (b) $|\text{BT departure}(i-1) - \text{BT departure}(i+1)| < \text{BT_Grad_Threshold}$;

- (c) $|\text{IBT departure}(i - \text{Interval}) - \text{BT departure}(i + 1)| < \text{BT_Grad_Threshold}$;

where i is the index of the ranked channel, Interval is the number of channels over which the gradient calculation is made, BT_Threshold denotes the threshold of BT and BT_Grad_Threshold represents the threshold of gradient of BT. All channels below this level are flagged cloud-affected and all channels above clear.

References

- Auligné T, McNally AP, Dee DP (2007) Adaptive bias correction for satellite data in a numerical weather prediction system. *Quart J R Meteorol Soc* 133:631–642
- Barker DM, Huang W, Guo YR, Bourgeois AJ, Xiao QN (2004) A three-dimensional variational data assimilation system for MM5: implementation and initial results. *Mon Weather Rev* 132:897–914
- Barker DM, Huang XY, Liu ZQ, Auligné T, Zhang X, Rugg S, Ajajj R, Bourgeois A, Bray J, Chen YS, Demirtas M, Guo YR, Henderson T, Huang W, Lin HC, Michalakes J, Rizvi S, Zhang XY (2012) The weather research and forecasting (WRF) model's community variational/ensemble data assimilation system: WRFDA. *Bull Am Meteorol Soc* 93:831–843
- Blumstein D, Chalon G, Carlier T, Buil C, Hébert Ph, Maciaszek T, Ponce G, Phulpin T, Tournier B, Siméoni D, Astruc P, Clauss A, Kayal G, Jegou R (2004) IASI instrument: technical overview and measured performances. *Proc SPIE* 5543:196–207
- Cavallo SM, Dudhia J, Snyder C (2011) A multilayer upper-boundary condition for longwave radiative flux to correct temperature biases in a mesoscale model. *Mon Weather Rev* 139:1952–1959
- Chen F, Dudhia J (2001) Coupling an advanced land-surface/hydrology model with the Penn State/NCAR MM5 modeling system. Part I: Model description and implementation. *Mon Weather Rev* 129:569–585
- Chou MD, Suarez MJ (1994) An efficient thermal infrared radiation parameterization for use in general circulation models. NASA Tech Memo, Maryland
- Collard AD, McNally AP (2009) The assimilation of Infrared Atmospheric Sounding Interferometer radiances at ECMWF. *Quart J R Meteorol Soc* 135:1044–1058
- Davis C, Wang W, Dudhia J, Torn R (2010) Does increased horizontal resolution improve hurricane wind forecasts? *Weather Forecast* 25:1826–1841
- Dee DP, Uppala SM (2009) Variational bias correction of satellite radiance data in the ERA-Interim reanalysis. *Quart J R Meteorol Soc* 135:1835–1841
- Dee DP, Uppala SM, Simmons AJ, Berrisford P, Poli P, Kobayashi S, Andrae U, Balmaseda MA, Balsamo G, Bauer P, Bechtold P, Beljaars ACM, van de Berg L, Bidlot J, Bormann N, Delsol C, Dragani R, Fuentes M, Geer AJ, Haimberger L, Healy SB, Hersbach H, Hólm EV, Isaksen L, Kallberg P, Köhler M, Matricardi M, McNally AP, Monge-Sanz BM, Morcrette JJ, Park BK, Peubey C, de Rosnay P, Tavalato C, Thepaut JN, Vitart F (2011) The ERA-interim reanalysis: configuration and performance of the data assimilation system. *Quart J R Meteorol Soc* 137:553–597
- Derber JC, Wu WS (1998) The use of TOVS clear-sky radiances in the NCEP SSI analysis system. *Mon Weather Rev* 126:2287–2299
- Eyre JR (1992) A bias correction scheme for simulated TOVS brightness temperatures. ECMWF, Reading
- Fiorino M (2009) Record-setting performance of the ECMWF IFS in medium-range tropical cyclone track prediction. *ECMWF Newsllett* 118:20–27
- Guidard V, Fourrié N, Brousseau P, Rabier F (2011) Impact of IASI assimilation at global and convective scales. *Quart J R Meteorol Soc* 137:1975–1987
- Han Y, Delst PV, Liu Q, Weng F, Yan B, Treadon R, Derber J (2006) JCSDA community radiative transfer model (CRTM)—version 1. NOAA Tech. Rep, Washington, DC
- Harris BA, Kelly G (2001) A satellite radiance-bias correction scheme for data assimilation. *Quart J R Meteorol Soc* 127:1453–1468
- Hong SY, Dudhia J, Chen SH (2004) A revised approach to ice microphysical processes for the bulk parameterization of clouds and precipitation. *Mon Weather Rev* 132:103–120
- Hong SY, Noh Y, Dudhia J (2006) A new vertical diffusion package with an explicit treatment of entrainment processes. *Mon Weather Rev* 134:2318–2341
- Hsiao LF, Liou CS, Yeh TC, Guo YR, Chen DS, Huang KN, Terng CT, Chen JH (2010) A vortex relocation scheme for tropical cyclone initialization in advanced research WRF. *Mon Weather Rev* 138:3298–3315
- Huang XY, Xiao Q, Barker DM, Xin Zhang, Michalakes J, Huang W, Henderson T, Bray J, Chen Y, Ma Z, Dudhia J, Guo YR, Xiaoyan Zhang, Won DJ, Lin HC, Kuo YH (2009) Four-dimensional variational data assimilation for WRF: formulation and preliminary results. *Mon Weather Rev* 137:299–314
- Ide K, Courtier P, Ghil M, Lorenc AC (1997) Unified notation for data assimilation: operational, sequential and variational. *J Meteorol Soc* 75:181–189
- Kain JS, Fritsch JM (1990) A one-dimensional entraining/detraining plume model and its application in convective parameterization. *J Atmos Sci* 47:2784–2802
- Li J, Liu H (2009) Improved hurricane track and intensity forecast using single field-of-view advanced IR sounding measurements. *Geophys Res Lett* 36:L11813. doi:10.1029/2009GL038285
- Liu Z, Rabier F (2002) The interaction between model resolution, observation resolution and observation density in data assimilation: a one-dimensional study. *Quart J R Meteorol Soc* 128:1367–1386
- Liu Q, Weng F (2006) Advanced doubling-adding method for radiative transfer in planetary atmosphere. *J Atmos Sci* 63:3459–3465
- Liu Z, Schwartz CS, Snyder C, Ha SY (2012) Impact of assimilating AMSU-A radiances on forecasts of 2008 Atlantic tropical cyclones initialized with a limited-area ensemble Kalman filter. *Mon Weather Rev* 140:4017–4034
- Lorenc AC (1986) Analysis methods for numerical weather prediction. *Quart J R Meteorol Soc* 112:1177–1194
- McNally T (2007) The use of satellite data in polar regions. In: ECMWF seminar proceedings on Polar Meteorology
- McNally AP, Watts PD (2003) A cloud detection algorithm for high-spectral-resolution infrared sounders. *Quart J R Meteorol Soc* 129:3411–3423
- McNally AP, Derber JC, Wu W, Katz BB (2000) The use of TOVS level-1b radiances in the NCEP SSI analysis system. *Quart J R Meteorol Soc* 126:689–724. doi:10.1002/qj.49712656315
- McNally AP, Watts PD, Smith JA, Engelen R, Kelly GA, Thepaut JN, Matricardi M (2006) The assimilation of AIRS radiance data at ECMWF. *Quart J R Meteorol Soc* 132:935–957
- Mlawer EJ, Taubman SJ, Brown PD, Iacono MJ, Clough SA (1997) Radiative transfer for inhomogeneous atmosphere: rRTM, a validated correlated-k model for the long-wave. *J Geophys Res* 102:16663–16682

- Parrish DF, Derber JC (1992) The National Meteorological Center's spectral statistical interpolation analysis system. *Mon Weather Rev* 120:1747–1763
- Prasad VS, Ramesh KJ, Bohra AK, Bhatia RC (1998) Assessment of quality and impact of full resolution TOVS temperature profile data on the operational global data assimilation–forecast system of India. *Meteorol Atmos Phys* 68:197–212
- Schwartz, CS, Liu Z, Huang XY, Kuo YH, Fong CT (2013) Comparing limited-area 3DVAR and hybrid variational–ensemble data assimilation methods for typhoon track forecasts: Sensitivity to outer loops and vortex relocation. *Mon Weather Rev* (in press)
- Schwartz CS, Liu Z, Chen Y, Huang XY (2012) Impact of assimilating microwave radiances with a limited-area ensemble data assimilation system on forecasts of typhoon Morakot. *Weather Forecast* 27:424–437
- Skamarock WC, Klemp JB, Dudhia J, Gill DO, Barker DM, Duda MG, Huang XY, Wang W, Powers JG (2008) A description of the advanced research WRF version 3. In: NCAR Tech Note, Boulder
- Wang X (2011) Application of the WRF hybrid ETKF-3DVAR data assimilation system for hurricane track forecasts. *Weather Forecast* 26:868–884
- Wang H, Huang XY (2012) TAMDAR observation assimilation in WRF 3D-Var and its impact on hurricane Ike (2008) forecast. *Atmos Ocean Sci Lett* 5:206–211
- Wang X, Barker DM, Snyder C, Hamill TM (2008) A Hybrid ETKF-3DVAR data assimilation scheme for the WRF model, Part I: Observing system simulation experiment. *Mon Weather Rev* 136:5116–5131
- Wang H, Mu M, Huang XY (2011) Application of conditional nonlinear optimal perturbation to tropical cyclone adaptive observation using the weather research forecasting (WRF) model. *Tellus A* 63:939–957
- Zapotocny TH, Jung JA, Marshall JFL, Treadon RE (2008) A two-season impact study of four satellite data types and rawinsonde data in the NCEP global data assimilation system. *Weather Forecast* 23:80–100
- Zhao K, Xue M, Lee WC (2012) Assimilation of GBVTD-retrieved winds from single-Doppler radar for short-term forecasting of Super Typhoon Saomai (0608) at landfall. *Quart J R Meteorol Soc* 138:1055–1071